Talanta 82 (2010) 1924–1928

Contents lists available at ScienceDirect

Talanta

journal homepage: www.elsevier.com/locate/talanta

Determination of trace amounts of mercury using hierarchically nanostructured europium oxide

Yanfen Peng, Xiaojun Chen, Zhiqiang Gao*

Institute of Bioengineering and Nanotechnology, 31 Biopolis Way, Singapore 138669, Singapore

ARTICLE INFO

Article history:
Received 18 May 2010
Received in revised form 10 August 2010
Accepted 10 August 2010
Available online 17 August 2010

Keywords:
Mercury
Europium oxide
Fluorescence spectrophotometry
Hierarchical nanostructure

ABSTRACT

This work reports a highly sensitive procedure for the determination of trace amounts of mercury, based on fluorescence quenching of thenoyltrifluoroacetone (TTA) capped hierarchically nanostructured europium oxide (cHN-Eu_2O_3). The HN-Eu_2O_3 consisted of nanometer-thick Eu_2O_3 sheets self-organized into nano- and micro-sized monoliths with a hierarchical architecture while retaining its desirable fluorescence properties. The fluorescence intensity of the cHN-Eu_2O_3 was 1000 times higher than that of commercial Eu_2O_3 nanoparticles (equivalent weight) when it was capped with TTA, suggesting that a synergetic effect, confining the longtime Eu^{3+} excitation within the nanostructure and light-harvesting effect of the capping agent, is responsible for this fluorescence enhancement. Excellent interaction between the cHN-Eu_2O_3 and solution species is expected owing to its large surface area, high surface-to-bulk ratio, and ultrahigh fluorescence intensity. As an example, aqueous suspensions of the cHN-Eu_2O_3 were used as sensing agent for the determination of trace amounts of mercury. A linear relationship between the concentration of mercury and fluorescence quenching was observed from 10 ppb to 10 ppm with a correlation coefficient of 0.997 and a detection limit of 5.0 ppb. Mercury in various samples was analyzed using the cHN-Eu_2O_3 suspension.

1. Introduction

Nanomaterials have attracted tremendous interest as these zero-dimensional nanoparticles [1] and quantum dots [2], one-dimensional nanotubes [3], nanowires [4], and nanoribbons [5] exhibit remarkable electronic, magnetic, optical, and catalytic properties that are distinctly different from their bulk counterparts [6,7]. In recent years, there has been a paradigm shift in the field of nanomaterials research, from synthesizing these nanoscale building blocks of arbitrary dimensions and morphologies to constructing three-dimensional (3D) hierarchical nanostructures with controllable architecture and functionality [6–8]. The formation of hierarchical nanostructures is generally considered to be a self-assembly process, in which building blocks self-assemble into regular higher level structures.

Europium oxide (Eu_2O_3), the stable sesquioxide of Eu^{3+} ion, has been employed extensively as an essential component phosphor in cathode-ray tube displays and as a fluorescent agent in light-emitting compounds [9]. Moreover, Eu_2O_3 is an attractive material for use in a variety of device size regimes, from nanoscale to macroscale due to its attractive fluorescence properties such as long emission lifetime, large Stokes shift and ultranarrow emission peaks [10–13]. Recent studies have sought to take advantage of those optical properties of Eu_2O_3 for implementation in nanoscale optical devices, such as nanocrystalline light-emitting diodes and biosensing agents [14,15]. We report herein, for the first time, the preparation of hierarchical nanostructures of Eu_2O_3 (HN-Eu_2O_3). These nanostructures consisted of nanometer-thick Eu_2O_3 sheets self-organized into nano- to micro-sized monoliths with a hierarchical architecture. The product obtained retained its desirable fluorescence properties that are typical of europium-based materials [9,16]. Unlike other fluorescent materials, for example quantum dots [17], the fluorescence properties of the HN-Eu_2O_3 originate from Eu^{3+} ion absorption are relatively unaffected by the size or the surface morphology of the material. Capping the HN-Eu_2O_3 with thenoyltrifluoroacetone (TTA) turned it into an ultrabright fluorescence sphere, noticeably visible under a fluorescence microscope. The cHN-Eu_2O_3 is of particular interest for applications in catalysis, energy conversion and storage, environmental abatement, and sensors. Attempts were made in applying the cHN-Eu_2O_3 in the determination of traces of mercury in environmental samples.

2. Experimental

Unless otherwise noted, solvents and chemicals were used as received from Sigma–Aldrich (St. Louis, MO). The HN-Eu_2O_3 was

* Corresponding author. Tel.: +65 68247113; fax: +65 64789085.
E-mail address: zqgao@ibn.a-star.edu.sg (Z. Gao).

0039-9140/$ – see front matter © 2010 Elsevier B.V. All rights reserved.
doi:10.1016/j.talanta.2010.08.011

synthesized by a simple one-step template-free procedure in aqueous solution. In a typical experiment, 0.10 g of europium acetate ($Eu(Ac)_3$) was dissolved into 25 ml of water, The solution was stirred with a magnetic stir bar and heated to 90 °C. A 1.0 ml aliquot of 20 mg/ml hexamethylenetetramine (HMT) was added dropwise. The clear mixture turned cloudy in 30 min, became opaque again after another 30 min, and some white precipitate was found at the bottom of the flask. Ninety minutes after the addition of HMT, the precipitate was collected and purified by multiple centrifugation–dispersion cycles with alcohol. This precursor was then calcinated at 500 °C for 3 h to obtain highly crystalline HN-Eu_2O_3. TTA capping was achieved by treating the HN-Eu_2O_3 with a saturated TTA solution in ethanol.

Transmission electron microscopic (TEM) experiments were performed on a FEI Tecnai G2 F20 electron microscope operated at 200 kV. Field-emission scanning electron microscopic (FESEM) experiments were conducted on a JEOL JSM-7400F electron microscope. UV–vis and fluorescence spectra were recorded on a V-570 UV/VIS/NIR spectrophotometer (JASCO Corp., Japan) and a Fluorolog®-3 spectrofluorometer (Jobin Yvon Inc, Edison, NJ), respectively. The quantum yield of the cHN-Eu_2O_3 was estimated by measuring integrated fluorescence intensities of the cHN-Eu_2O_3 sample and the reference $(Eu(TTA)_3(phen)$ in DMF, QY = 36.5%) under 380 nm excitation [18]. Fluorescence images of the cHN-Eu_2O_3 were acquired with an Olympus Inverted Microscope. Brunauer–Emmett–Teller (BET) surface area was obtained using a Micromeritics ASAP 2020 M system.

Mercury analysis: for each sample three replicates of approximately 0.50 g were transferred to 25 ml polypropylene test tubes. To each replicate 5.0 ml of 3:1 (w/w) H_2SO_4:HNO_3 was added and the mixture was heated to 80 °C for 120 min. Then 10.0 ml of 6 M HCl and 3.0 ml of 0.1 M $KBrO_3$/KBr solution were added. After mixing, the sample was heated to 60 °C in a water bath overnight. The sample solution was yellow in color and clear without any precipitate. Next, 1.0 M hydroxylamine hydrochloride was slowly added until the solution becomes colorless. For spiked samples, Hg^{2+} calibration standards were added to the polypropylene test tubes before digestion. Water samples were filtered through a P10 glass filter prior to digestion. To a suitable aliquot of sample solution added 1.0 μg/ml cHN-Eu_2O_3. After equilibrating at room temperature for 30 min under stirring, the fluorescence of each mixture was measured. For control experiments, the same procedure was applied, except that blank 0.10 M $NaNO_3$ solution used instead of the mercury sample solution.

3. Results and discussion

Fig. 1a is a FESEM image of the HN-Eu_2O_3, showing uniform spherical particles with a diameter of ~1 μm. Energy dispersive X-ray analysis indicated that the particles are essentially pure Eu_2O_3. A high-magnification FESEM image (Fig. 1, insert) revealed that the spherical particles are actually built from several dozen nanosheets with smooth surfaces. These nanosheets, with a thickness of 2–5 nm, are interconnected to each other to form hierarchical nanostructures. Crystalline grains in TEM micrographs (Fig. 1b) and a series of diffraction rings in a selected-area electron diffraction experiment indicated that the HN-Eu_2O_3 is essentially polycrystalline. Depending on the particle size, BET surface area was found to be from 180 to 230 m^2/g, which is comparable to those of other metal oxide-based HN-particles [8]. Smaller HN-Eu_2O_3 spheres down to 200 nm can be prepared with higher $Eu(Ac)_3$ concentrations while keeping the $Eu(Ac)_3$/HMT ratio unchanged.

Fig. 2a shows UV–vis absorption spectra of the HN-Eu_2O_3 before and after the TTA capping. For comparison, the UV–vis spectrum of TTA in water is also given in Fig. 2a (trace 3). The spectrum of

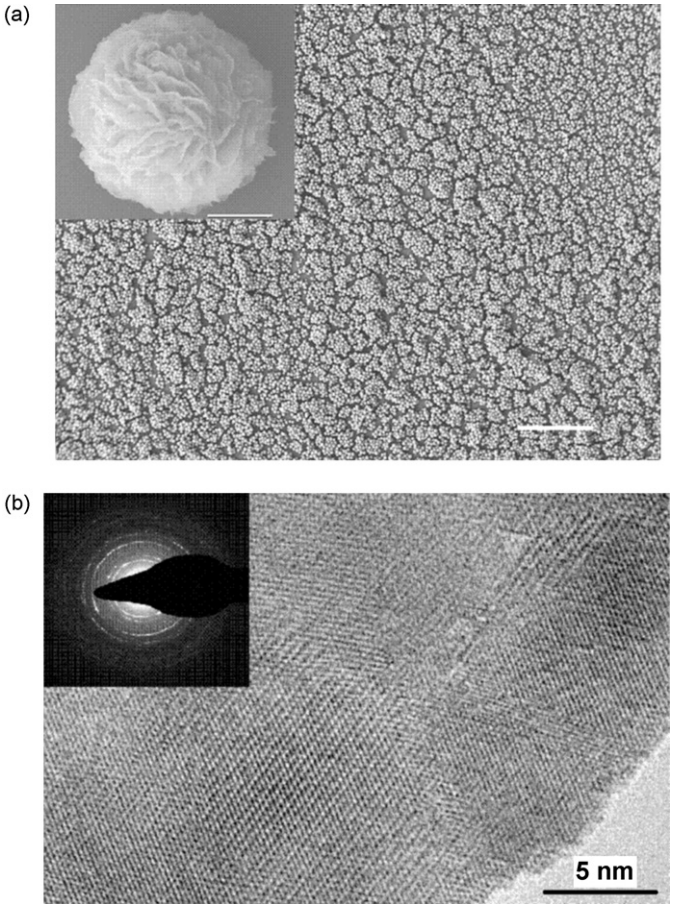

Fig. 1. (a) Representative FESEM images of the HN-Eu_2O_3 at low magnification (scale bar 20 μm) and at high magnification (insert, scale bar 0.5 μm). (b) A high resolution TEM image of HN-Eu_2O_3 and the corresponding SAED pattern (insert).

the HN-Eu_2O_3 before capping was more or less characteristic of the spectrum of nanoparticulate Eu_2O_3: a rather broad absorption band stretches over 350 nm (Fig. 2a, trace 2). The principal features were two absorption peaks at 230 and 270 nm, which correspond to transitions from the $^7F_0$ ground state to charge transfer states due to europium–oxygen interaction. [19]. The long absorption tail is due to scattering by the HN-Eu_2O_3 spheres [20]. The spectrum of the cHN-Eu_2O_3 appeared not as a simple superposition of TTA and the HN-Eu_2O_3, but as a superposition of the HN-Eu_2O_3 and an europium–TTA complex (Fig. 2a, trace 1) with a main absorption peak in the 300–400 nm region [21], indicating that TTA is co-ordinatively grafted onto the HN-Eu_2O_3. Due to the hierarchical nature of the nanostructure and the ultrathin nanosheet building blocks, a very large portion of Eu_2O_3 is located on the surface, capping with TTA inevitably alerts the chemical environment for most of Eu_2O_3.

The excited states of Eu^{3+} are known to be very sensitive to water. Water molecules in the first co-ordination sphere of Eu^{3+} provide an efficient route for radiationless deactivation, which is particularly efficient in co-ordinatively unsaturated systems [22]. As expected, no Eu^{3+} emission was visible in the as-obtained HN-Eu_2O_3 in water under UV-irradiation (Fig. 2c, insert). On the other hand, upon capping, the water molecules on the HN-Eu_2O_3 surface were displaced by TTA, leading to the formation of a TTA outlayer. This TTA outlayer acts not only as a water repelling layer, but also as an efficient light-harvesting layer by its well-known antenna effect [23]. The substitution of H_2O by TTA on the HN-Eu_2O_3 surface effectively removes the nonradiative decays caused by weak couplings of the Eu^{3+} excited states with the OH oscilla-

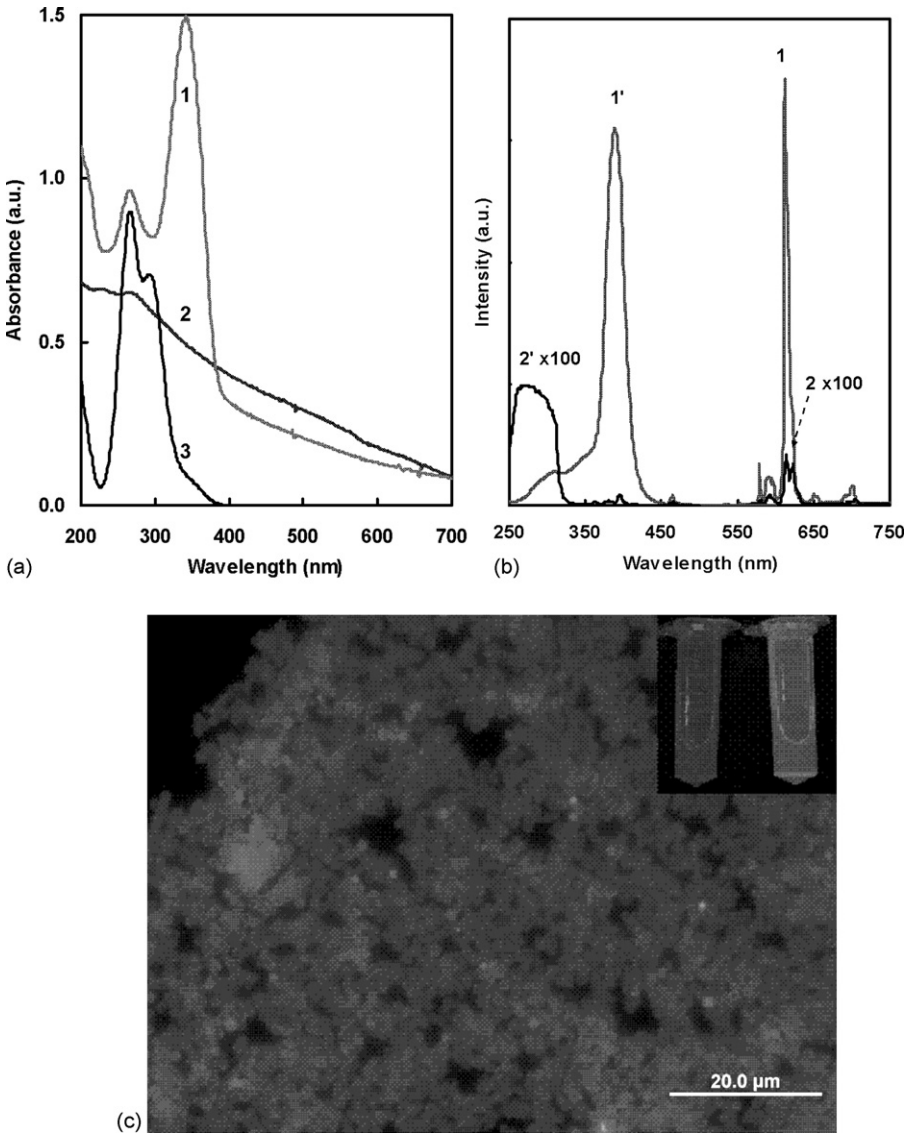

Fig. 2. (a) UV absorption spectra of (1) 10 μg/ml the cHN-Eu_2O_3, (2) 10 μg/ml the HN-Eu_2O_3 and (3) 10 μg/ml TTA in water. (b) (1) Emission and (1′) excitation spectra of the cHN-Eu_2O_3; (2) emission and (2′) excitation spectra of Eu_2O_3 nanoparticles, and (c) a typical fluorescence image of the cHN-Eu_2O_3 taken under UV illumination. Insert: photographs, taken under a UV lamp (left) before and (right) after the TTA capping.

tors, resulting in a dramatic increase in the fluorescence intensities. As illustrated in Fig. 2c, the red fluorescence of cHN-Eu_2O_3 was so intensive that individual HN-Eu_2O_3 spheres were clearly visible in the solid state under a fluorescence microscope. The red emission from cHN-Eu_2O_3 was also readily visible to the naked eye upon excitation with a UV lamp (Fig. 2c, insert). Up illumination, the capping layer is excited and then decays rapidly to its lowest triplet state. And more importantly, the majority of Eu_2O_3 is able to receive the energy transferred from the excited TTA due again to the unique hierarchical structure and ultrathin nanosheet building blocks. In addition, the typical red emission of the cHN-Eu_2O_3 indicates that the Eu^{3+} emitting center does not occupy a center of symmetry. If the Eu^{3+} center were at the center of symmetry, then the emission should appear orange [24]. This intensive Eu^{3+} emission was further investigated by fluorescence spectrophotometry. The emission spectrum of the cHN-Eu_2O_3 (Fig. 2b, trace 1) displayed the characteristic $^5D_0$–^7F_J (J ¼ 0–4) transitions of Eu^{3+} under excitation from $^7F_0$ to $^5L_6$ level [16], or under ligand excitation. The hypersensitive $^5D_0$–$^7F_2$ transition is predominant in all cases, suggesting that Eu^{3+} ions lie in a non-centrosymmetrical environment [16]. In the spectrum, there was no evidence of emissions from the triplet state of TTA, implying that there is an efficient energy transfer from the triplet state of TTA to the HN-Eu_2O_3. It is well-known that the magnetic–dipole transitions $^5D_0$–$^7F_1$ are nearly independent of the ligand field, and therefore can be used as an internal standard to account for ligand difference [25]. The electric–dipole transitions $^5D_0$–$^7F_{J=2,4,6}$, the so-called hypersensitive transitions, are sensitive to the symmetry of the co-ordination sphere. The intensity ratio of the magnetic–dipole transition to the electric–dipole transition in the europium complex measures the symmetry of the co-ordination sphere [23,26]. The intensity ratios of the $^5D_0$–$^7F_2$ transition to the $^5D_0$–$^7F_1$ transition in pure Eu_2O_3 nanoparticles (30–50 nm, from Nanostructured & Amorphous Materials, Inc. Houston, TX 77084) and the cHN-Eu_2O_3 were determined to be 11.5 and 13.5, respectively. These results show that Eu^{3+} ions in the cHN-Eu_2O_3 exhibit different local environments because of the influence of the surrounding TTA molecules. As seen in Fig. 2b traces 1 and 2, the fluorescence intensity the cHN-Eu_2O_3 was more than 1000 times higher than that of the commercial Eu_2O_3 nanoparticles (equivalent weight) and ~28 higher

than that of the commercial Eu_2O_3 nanoparticles coated with TTA. The emission life time and quantum yield of the cHN-Eu_2O_3 were found to be ~1.0 ms and ~68%, respectively.

The excitation spectrum (Fig. 2b, trace 1′) of the cHN-Eu_2O_3 displays a predominant TTA ligand excitation band at 390 nm, as a result of the antenna effect [24], while the excitation spectrum of the Eu_2O_3 nanoparticles was given as a reference (Fig. 2b, trace 2′). Moreover, the absorption spectrum revealed that the excitation bands are displaced to lower energies when compared to the absorption bands of the free ligand (Fig. 2a, trace 3), indicating the co-ordinative nature of TTA with Eu^{3+} ion. It was clearly observable that the cHN-Eu_2O_3 is strongly excitable over all the low-energy ultraviolet region of the spectrum. In addition, in the excitation spectrum of the HN-Eu_2O_3, the ^7F–^5D inner-shell excitation lines at 465 nm persists, suggesting that the f–f inner-shell transitions are largely unaffected and there is very little of quenching through non-radiative energy transfer from the excited state to the TTA capping layer.

Potential applications of hierarchically nanostructured materials include catalysis, energy conversion and storage, environmental abatement, and sensors. The highly intensive fluorescence, in combination with the networks formed by the interconnected nanosheets, producing multiscale porosity, high surface-to-bulk ratio, and ultralarge surface area, makes the cHN-Eu_2O_3 a good candidate for heavy metals removal and possibly an ideal sensing material for probing the heavy metals simultaneously. Indeed, it was observed that traces of mercury effectively quench the fluorescence of the cHN-Eu_2O_3, leading to potential applications in the determination of mercury. The ability of the cHN-Eu_2O_3 to detect mercury was then investigated by adding successive aliquots of aqueous solutions of mercury to aqueous suspensions of the cHN-Eu_2O_3 and monitoring the changes in fluorescence intensity (Fig. 3a). The fluorescence of the cHN-Eu_2O_3 was completely quenched by mercury at concentrations higher than 20 ppm. Quenching efficiencies were fit to the Stern–Volmer equation, $I_0/I = K_{sv}[A] + 1$ [27], where I is the fluorescence intensity, I_0 is the intensity at $[A] = 0$, and K_{SV} is the Stern–Volmer constant. A plot of mercury quenching efficiency was linear up to 10 ppm, at which point there was a gradual decrease in quenching efficiency (Fig. 3b). This nonlinear relationship observed may indicate saturation of the surface binding sites. The selectivity of the cHN-Eu_2O_3 was tested by performing quenching experiments at 1.0 ppm Hg^{2+} in the presence of common metal ions. As shown in Fig. 4, the fluorescence intensity of the cHN-Eu_2O_3 was little affected by the presence of 10 ppm of Ca^{2+}, Fe^{2+}, Fe^{3+}, Cu^{2+}, Mg^{2+}, Ni^{2+}, Co^{2+}, Al^{3+}, Zn^{2+}, and Mn^{2+}. However, it was observed that the fluorescence intensity was reduced by 15% in the presence of 10 ppm Pb^{2+} and it was almost completely quenched when Pb^{2+} concentration was increased to 50 ppm, implying some interference from Pb^{2+}. Better selectivity was observed when the determination of mercury was carried out in the presence of 50 μM phytic acid (masking agent), due to the fact that phytic acid forms stable complexes with many metal ions, including Fe^{2+}, Cu^{2+}, Ni^{2+}, Co^{2+}, Zn^{2+}, and Pb^{2+} [28]. For example, the cHN-Eu_2O_3 produced ~8-fold higher selectivity toward Hg^{2+} ions over the other metal ions when mercury was analyzed in solutions containing 50 μM phytic acid.

The proposed method was applied to the determination of mercury by the single standard addition method. The samples were digested and separated using the procedure recommended by Marczenko [29]. A 50 mM $NaNO_3$ solution was used as the medium for mercury sample preparation. As seen in Table 1, good agreement between the proposed method and atomic adsorption spectrometry (AAS) was obtained. A relative standard deviation of 10% was obtained for six determinations of 100 ppb mercury. The recoveries obtained (94–103%) were also good enough for practical use.

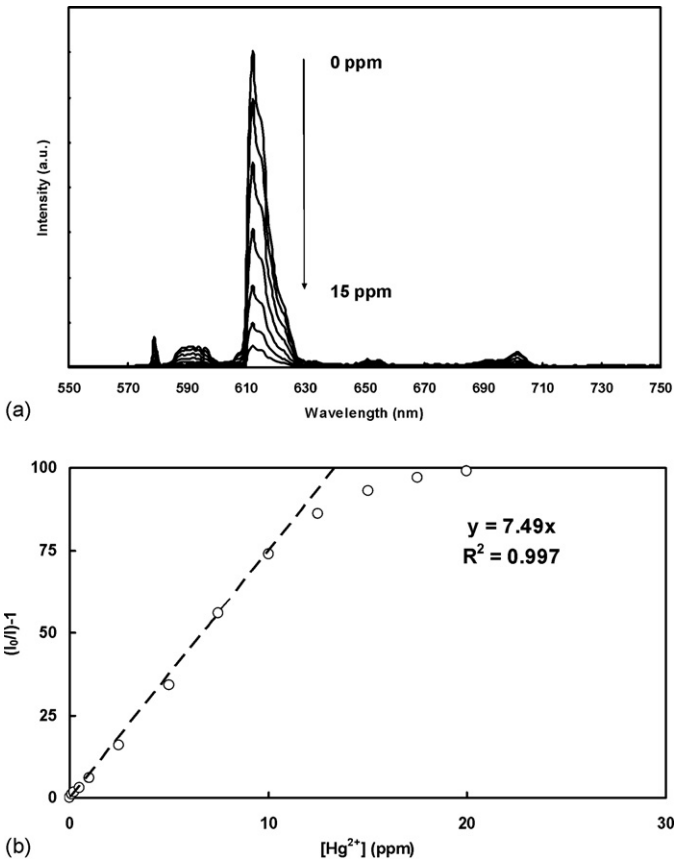

Fig. 3. (a) Changes in the emission of the cHN-Eu_2O_3 (excited at 380 nm) in the presence of increasing amounts of mercury in 2.5 ppm increments and (b) a plot of the relative intensity vs. mercury added.

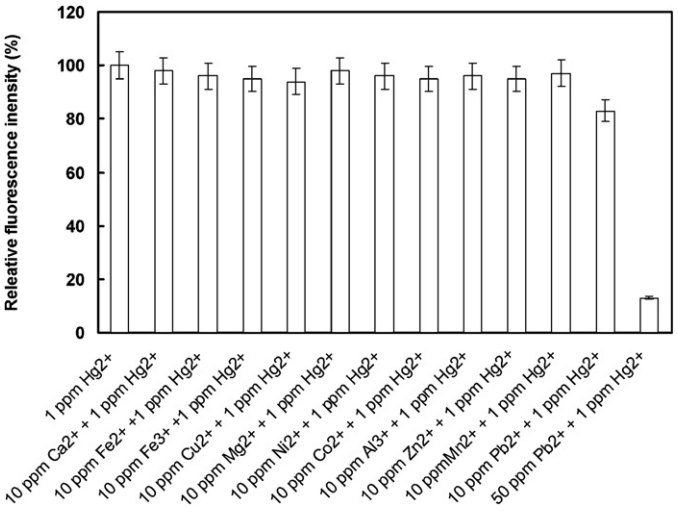

Fig. 4. Effect of common metal ions on the determination of 1.0 ppm mercury. Experimental conditions are as for Fig. 3.

Table 1
Results of mercury analysis ($n = 6$).

Sample	Found (this method) (μg/g)	Found (AAS) (μg/g)
Hair	0.33	0.29
Shell fish	0.130	0.120
Fish	0.232	0.235
Waste water	0.093	0.090

4. Conclusion

In summary, we have developed a fluorescence quenching procedure for sensitive determination of mercury using the cHN-Eu_2O_3. The HN-Eu_2O_3 was synthesized by a simple one-step template-free process. Capping the HN-Eu_2O_3 with TTA resulted in an enormous enhancement in fluorescence, which is much more intensive than that of commercial Eu_2O_3 nanoparticles under the same conditions. The excellent fluorescence properties of the cHN-Eu_2O_3 are related to their special structural uniqueness and imply potential applications in catalysis, energy conversion, and sensing. The cHN-Eu_2O_3 was then utilized to determine trace amounts of mercury in various samples. Further studies will focus on extending to the synthesis of hierarchical nanostructures and their applications.

Acknowledgements

The authors thank Dr. Han Yu for his assistance with TEM studies. This work was funded by the Institute of Bioengineering and Nanotechnology A*STAR.

References

[1] B.L. Cushing, V.L. Kolesnicheko, C.J. O'Connor, Chem. Rev. 104 (2004) 3893–3946.
[2] M. Nirmal, L. Brus, Acc. Chem. Res. 32 (1999) 407–414.
[3] S. Iijima, Nature 354 (1991) 56–58.
[4] M.P. Zach, K.H. Ng, R.M. Penner, Science 290 (2000) 2120–2123.
[5] Z.W. Pan, Z.R. Dai, Z.L. Wang, Science 291 (2001) 1947–1949.
[6] C. Burda, X.B. Chen, R. Narayanan, M.A. El-Sayed, Chem. Rev. 105 (2005) 1025–1102.
[7] H. Colfen, M. Antonietti, Angew. Chem. Int. Ed. 44 (2005) 5576–5591.
[8] J. Hu, L. Zhong, W. Song, L. Wan, Adv. Mater. 20 (2008) 2977–2982.
[9] W.M. Yen, S. Shionoya, H. Yamamoto, Practical Applications of Phosphors, CRC Press, New York, 2006.
[10] D. Parker, Chem. Soc. Rev. 33 (2004) 156–165.
[11] D. Parker, R.S. Dickins, H. Puschmann, C. Crossland, J.A.K. Howard, Chem. Rev. 102 (2002) 1977–2010.
[12] J.-C.G. Bunzli, C. Piguet, Chem. Rev. 102 (2002) 1897–1928.
[13] N. Sabbatini, M. Guardigli, J.-M. Lehn, Coord. Chem. Rev. 123 (1993) 201–228.
[14] J. Feng, G. Shan, A. Maquieira, M.E. Koivunen, B. Guo, B.D. Hammock, I.M. Kennedy, Anal. Chem. 75 (2003) 5282–5286.
[15] M. Nichkova, D. Dosev, S.J. Gee, B.D. Hammock, I.M. Kennedy, Anal. Chem. 77 (2005) 6864–6873.
[16] G. Blasse, B.C. Grabmaier, Luminescent Materials, Springer-Verlag, Berlin, Germany, 1994.
[17] U. Resch-Genger, M. Grabolle, S. Cavaliere-Jaricot, R. Nitschke, T. Nann, Nat. Methods 5 (2008) 763–775.
[18] N. Filipescu, G.W. Mushrush, C.R. Hurt, N. McAvory, Nature 211 (1966) 960–961.
[19] M. Yin, W. Zhang, S. Xia, J.C. Krupa, J. Lumin. 68 (1996) 335–339.
[20] J. Nanda, S. Sapra, D.D. Sarma, N. Chandrasekharan, G. Hodes, Chem. Mater. 12 (2000) 1018–1024.
[21] X.P. Fan, Z.Y. Wang, M.Q. Wang, J. Lumin. 99 (2002) 247–254.
[22] J.P. Leonard, C.M.G. Dos Santos, S.E. Plush, T. McCabe, T. Gunnlaugsson, Chem. Commun. (2007) 129–131.
[23] A.M. Klonkowski, S. Lis, M. Pietraszkiewicz, Z. Hnatejko, K. Czarnobaj, M. Elbanowski, Chem. Mater. 15 (2003) 656–663.
[24] G. Wakefield, H.A. Keron, P.J. Sobson, J.L. Hutchison, J. Colloid Interface Sci. 215 (1999) 179–182.
[25] J.-C.G. Bunzli, G.R. Choppin (Eds.), Lanthanide Probes in Life, Chemical and Earth Sciences, Theory and Practice, Elsevier, New York, 1989, pp. 102–103.
[26] A.F. Kirby, D. Foster, F.S. Richardson, Chem. Phys. Lett. 95 (1983) 507–509.
[27] J.G. Calvert, J.N. Pitts, Photochemistry, John Wiley & Sons, Inc., New York, 1966, pp. 663–670.
[28] E. Vasca, S. Materazzi, T. Caruso, O. Milano, C. Fontanella, C. Manfredi, Anal. Bioanal. Chem. 374 (2002) 173–178.
[29] Z. Marczenko, Spectrophotometric Determination of Elements, Halstead Press, New York, 1976, pp. 351–355.